Versatile endless optical polarization controller/tracker/demultiplexer

Benjamin Koch,[1,2,*] Reinhold Noé,[1,2] David Sandel,[1] and Vitali Mirvoda[1]

[1]*University of Paderborn, EIM-E, Warburger Str. 100, 33098 Paderborn, Germany*
[2]*Novoptel GmbH, EIM-E, Warburger Str. 100, 33098 Paderborn, Germany*
[*]*koch@ont.upb.de*

Abstract: Following an initial discussion of control error signal generation, we present new developments and applications of automatic endless optical polarization control based on a commercial electrooptic $LiNbO_3$ polarization transformer: (i) Fast tracking and subsequent demultiplexing of DPSK/DQPSK/QAM polarization channels was hitherto limited to a fairly fixed optical input power. With APD photoreceivers used for residual interference detection, we demonstrate here an optical level tolerance of at least 7 dB, compared to only 3 dB for PIN photoreceivers. DPSK channel polarizations are tracked at up to 40 krad/s and higher speed on the Poincaré sphere. (ii) High-order optical modulation schemes require increased accuracy of the polarization controller in the demultiplexer. This is possible at the expense of a reduced tracking speed. We achieve a mean polarization extinction ratio of >40 dB or <0.02 rad error while tracking arbitrary endless polarization changes of up to 1000 rad/s. (iii) While electronic polarization tracking in coherent receivers is currently limited to a symbol rate of about 28 GBaud we show optical polarization tracking of a signal with 1 THz bandwidth.

OCIS codes: (060.4510) Optical communications; (130.3730) Lithium niobate; (260.5430) Polarization.

References and links

1. P. Krummrich, "Field trial results on statistics of fast polarization changes in longhaul WDM transmission systems," Proc. OFC/NFOEC2005, OThT6, March 6–11, 2005, Anaheim, CA, USA.
2. M. Reimer, D. Dumas, G. Soliman, D. Yevick, and M. O'Sullivan, "Polarization evolution in dispersion compensation modules," Proc. OFC/NFOEC 2009, San Diego, CA, Mar. 22–26, 2009, Paper OWD.
3. B. Koch, R. Noé, V. Mirvoda, and D. Sandel, "100-krad/s endless polarisation tracking with miniaturised module card," Electron. Lett. **47**(14), 813–814 (2011).
4. Ciena Wavelogic 3, application note available on 11 Oct. 2013 at http://www.ciena.com/resources/application-notes/Enabling-a-Bigger-and-Smarter-Network-with-Cienas-WaveLogic-3-AN.html.
5. B. Koch, R. Noé, V. Mirvoda, D. Sandel, V. Filsinger, and K. Puntsri, "40-krad/s Polarization tracking in 200-Gb/s PDM-RZ-DQPSK transmission over 430 km," IEEE Photonics Technol. Lett. **22**(9), 613–615 (2010).
6. B. Koch, R. Noé, V. Mirvoda, H. Griesser, S. Bayer, and H. Wernz, "Record 59-krad/s polarization tracking in 112-Gb/s, 640-km, PDM-RZ-DQPSK transmission," IEEE Photonics Technol. Lett. **22**(19), 1407–1409 (2010).
7. B. Koch, R. Noe, D. Sandel, V. Mirvoda, J. Omar, and K. Puntsri, "20-Gb/s PDM-RZ-DPSK transmission with 40 krad/s endless optical polarization tracking," IEEE Photonics Technol. Lett. **25**(9), 798–801 (2013).
8. P. S. Cho, G. Harston, C. J. Kerr, A. S. Greenblatt, A. Kaplan, Y. Achiam, G. Levy-Yurista, M. Margalit, Y. Gross, and J. B. Khurgin, "Investigation of 2-b/s/Hz 40-gb/s DWDM transmission over 4×100 km SMF-28 fiber using RZ-DQPSK and polarization multiplexing," IEEE Photonics Technol. Lett. **16**(2), 656–658 (2004).
9. P. Boffi, M. Ferrario, L. Marazzi, P. Martelli, P. Parolari, A. Righetti, R. Siano, and M. Martinelli, "20-Gb/s PolDM duobinary transmission over 350-km SSMF supported by a polarization stabilizer and an optical dispersion compensator," IEEE Photonics Technol. Lett. **20**(13), 1118–1120 (2008).
10. A. R. Chraplyvy, A. H. Gnauck, R. W. Tkach, J. L. Zyskind, J. W. Sulhoff, A. J. Lucero, Y. Sun, R. M. Jopson, F. Forghieri, R. M. Derosier, C. Wolf, and A. R. McCormick, "1-Tb/s transmission experiment," IEEE Photonics Technol. Lett. **8**(9), 1264–1266 (1996).
11. Z. N. Wang and C. J. Xie, "Automatic optical polarization demultiplexing for polarization division multiplexed signals," Opt. Express **17**(5), 3183–3189 (2009).

#204307 - $15.00 USD Received 6 Jan 2014; revised 13 Feb 2014; accepted 13 Feb 2014; published 1 Apr 2014

12. M. I. Hayee, M. C. Cardakli, A. B. Sahin, and A. E. Willner, "Doubling of bandwidth utilization using two orthogonal polarizations and power unbalancing in a polarization-division-multiplexing scheme," Photonics Technol. Lett. **13**(8), 881–883 (2001).
13. S. Bhandare, D. Sandel, B. Milivojevic, A. Hidayat, A. Fauzi Abas Ismail, H. Zhang, S. Ibrahim, F. Wüst, and R. Noé, "5.94 Tbit/s, 1.49 bit/s/Hz (40×2×2×40 Gbit/s) RZ-DQPSK polarization division multiplex C-Band transmission over 324 km," IEEE Photonics Technol. Lett. **17**, 914–916 (2005).
14. H. Masuda, A. Sano, T. Kobayashi, E. Yoshida, Y. Miyamoto, Y. Hibino, K. Hagimoto, T. Yamada, T. Furuta, and H. Fukuyama, "20.4-Tb/s (204 × 111 Gb/s) transmission over 240 km using bandwidth-maximized hybrid Raman/EDFAs," PDP20, OFC 2007, March 25, 2007, Anaheim, California, USA.
15. A. H. Gnauck, G. Charlet, P. Tran, P. Winzer, C. Doerr, J. Centanni, E. Burrows, T. Kawanishi, T. Sakamoto, and K. Higuma, "25.6-Tb/s C+L-band transmission of polarization-multiplexed RZ-DQPSK signals," PDP19, OFC 2007, March 25, 2007, Anaheim, California, USA.
16. J.-X. Cai, O. V. Sinkin, C. R. Davidson, D. G. Foursa, A. J. Lucero, M. Nissov, A. N. Pilipetskii, W. W. Patterson, and N. S. Bergano, "40 Gb/s transmission using polarization division multiplexing (PDM) RZ-DBPSK with automatic polarization tracking," OFC2008, paper PDP4, San Diego, CA, USA, February 24–28, 2008.
17. X. S. Yao, L.-S. Yan, B. Zhang, A. E. Willner, and J. Jiang, "All-optic scheme for automatic polarization division demultiplexing," Opt. Express **15**(12), 7407–7414 (2007).
18. Y. Shen, X. Liu, S. Zhong, L. Zong, J. Veselka, P. Kim, J. Ferment, and H. P. Sardesai, "Design of polarization de-multiplexer and PMD compensator for 112 Gb/s direct-detect PDM RZ-DQPSK systems," J. Lightwave Technol. **28**, 3282–3293 (2010).
19. J. Zhang, X. Yuan, M. Lin, T. Jinjing, Y. Zhang, M. Zhang, and X. Zhang, "Transmission of 112Gb/s PM-RZ-DQPSK over 960km with adaptive polarization tracking based on power difference," Proc. ECOC 2010, P2.09.
20. M. Yagi, S. Satomi, and S. Ryu, "Field Trial of 160-Gbit/s, Polarization-division multiplexed RZ-DQPSK transmission system using automatic polarization control," Proc. OFC/NFOEC 2008, San Diego, CA, Feb. 24–28, 2008, Paper OThT7.
21. T. Ito, S. Fujita, E. T. de Gabory, and K. Fukuchi, "Improvement of PMD Tolerance for 110 Gb/s Pol-Mux RZ-DQPSK Signal with optical pol-dmux using optical PMD compensation and asymetric symbol-synchronous chirp," Proc. OFC/NFOEC 2009, San Diego, CA, Mar. 22–26, 2009, Paper OThR5.
22. H. Wernz, S. Herbst, S. Bayer, H. Griesser, E. Martins, C. Fuerst, B. Koch, V. Mirvoda, R. Noé, A. Ehrhardt, L. Schuerer, S. Vorbeck, M. Schneiders, D. Breuer, and R. P. Braun, "Nonlinear behaviour of 112 Gb/s polarisation-multiplexed RZ-DQPSK with direct detection in a 630 km field trial," Proc. European Conference on Optical Communication (ECOC2009), Tu3.4.3, Vienna, Austria, 20-24 Sept. 2009.
23. R. Noé, H. Heidrich, and D. Hoffmann, "Endless polarization control systems for coherent optics," J. Lightwave Technol. **6**(7), 1199–1207 (1988).
24. N. G. Walker and G. R. Walker, "Polarization control for coherent optical communications," J. Lightwave Technol. **8**(3), 438–458 (1990).
25. F. Heismann and M. S. Whalen, "Fast automatic polarization control system," IEEE Photonics Technol. Lett. **4**(5), 503–505 (1992).
26. R. Nagarajan, M. Kato, J. Pleumeekers, D. Lambert, V. Lal, A. Dentai, M. Kuntz, J. Rahn, H.-S. Tsai, R. Malendevich, G. Goldfarb, J. Tang, J. Zhang, T. Butrie, M. Raburn, B. Little, A. Nilsson, M. Reffle, F. Kish, and D. Welch, "10 channel, 45.6Gb/s per channel, polarization multiplexed DQPSK InP receiver photonic integrated circuit", Proc. OFC 2010, PDP B2, 21–25 March 2010, San Diego, USA.
27. http://www.novoptel.de/Control/EPC1000_application_note_01.pdf, downloaded 30 Dec. 2013.
28. R. Noé, S. Hinz, D. Sandel, and F. Wust, "Crosstalk detection schemes for polarization division multiplex transmission," J. Lightwave Technol. **19**(10), 1469–1475 (2001).

1. Introduction

For fiberoptic communication with high spectral efficiency, the two independent polarization modes of a singlemode fiber must be exploited. Polarization in optical fiber can sometimes vary quite fast [1,2], and the communication systems should be able to track this.

Polarization can be controlled in a variety of applications. In the simplest case, the optical signal is unmodulated [3]. Related to this is polarization control in a single-polarization coherent receiver. This was the initial driver for polarization control research. Nowadays, a main driving source for polarization control is polarization division multiplex (PDM) of modulated data signals, which doubles fiber capacity compared to the traditional single-polarization systems. Coherent polarization-diversity detection is a powerful technology for receiving such signals [4], since it offers compensation of the linear distortion polarization mode dispersion (PMD and chromatic dispersion (CD). In a number of transmission scenarios with state-of-the-art low-PMD fiber, PMD compensation is not needed. Also, CD can be compensated optically. Even though, the symbol rate of coherent systems is currently limited to 28 Gbaud. This is due to the electronic bottleneck presented by ultrafast few-bit analog-to-digital converters (ADCs). In contrast, PDM-DQPSK with 50 Gbaud can be demultiplexed

#204307 - $15.00 USD Received 6 Jan 2014; revised 13 Feb 2014; accepted 13 Feb 2014; published 1 Apr 2014

optically already since a couple of years [5]. Furthermore, the one-bit ADCs of such receivers and the absence of digital signal processing greatly reduces power consumption. Other similar experiments are [6–22]. Older experimental works about electrooptic, hence potentially fast polarization control are [23–25]. With appropriate extra effort, electronic polarization control is possible not only in coherent but also in incoherent receivers [26].

We present how, depending on the application, the error signals for optical polarization controllers can be obtained (Section 2).

A practical restriction in recent PDM systems with fast optical polarization control and demultiplexing [5–7] was the need for a fairly fixed optical power level. If, during operation, the optical input power was not controlled, then a power increase made control unstable while a power decrease reduced the polarization tracking speed almost proportionally. Fast tracking and subsequent demultiplexing of DPSK/DQPSK/QAM polarization channels hence needed the optical input power to be stabilized. As a remedy we use avalanche photodiode (APD) frontends in the residual interference detector (Section 3). An APD voltage source with negative impedance makes the detected interference signal to first order independent of optical power. Variations of demultiplexer input power in a 9-dB range leave tracking performance in a 20-Gb/s, 430-km PDM-DPSK system fairly unaffected.

Reports from other researchers about achieved extinction under automatic polarization control are scarce, even though the value 14 dB (= 4%) of the early work [25] has probably been surpassed meanwhile. In our own experiments we have achieved a mean extinction of about 29.5 dB [6] at 50 krad/s tracking speed. However, even higher extinction is needed for higher-order PDM-QAM or similar modulation schemes. In midrange transmission scenarios, where ultimate OSNR performance is not needed, these are increasingly discussed. While such schemes could hitherto be detected only in coherent polarization-diversity receivers we show here that optical polarization tracking is possible with a mean polarization extinction ratio of >40 dB or <0.02 rad error on the Poincaré sphere (Section 4). This comes at the expense of a tracking speed reduction to 1000 rad/s.

As mentioned, a fundamental limit of coherent receivers is the limited electronic bandwidth. Whatever the achievable symbol rate is for the detection of binary symbols, it will be lower for analog-to-digital converters with several bit resolution. Here the huge bandwidth of optical polarization control technology comes into play. We extend the bandwidth of endless optical polarization control much beyond earlier reported values to 1 THz (Section 5).

Conclusions are found at the end of this paper (Section 6).

2. Error signal generation

Since a synopsis of error signal generation methods for polarization control seems not to be available in the scientific literature we provide this here, based on our description [27].

2.1 Optical power of cross-polarized signal

Figure 1 shows the block diagram of a polarization control system for a – usually unmodulated – single-polarization signal. It is passed through an electrooptic $LiNbO_3$ polarization transformer and a subsequent polarization beamsplitter (PBS). The simplest way of determining polarization mismatch errors is to measure the optical power of the cross-polarized signal at the second PBS output.

Let $\mathbf{E}_S$ be the normalized optical field vector of the optical wave behind the $LiNbO_3$ polarization transformer, before an ideal PBS or polarizer with normalized transmitted eigenmode $\mathbf{E}_{pol,1}$. The relative intensity *RI* or normalized output power equals $RI = \left|\mathbf{E}_{pol,1}^{+}\mathbf{E}_S\right|^2$. The + sign means Hermitian conjugate. The relative intensity error is $RIE = 1 - RI = \left|\mathbf{E}_{pol,2}^{+}\mathbf{E}_S\right|^2$, i.e. the normalized power of the cross-polarized output signal, where $\mathbf{E}_{pol,2}$ is the second polarizer eigenmode, orthogonal to $\mathbf{E}_{pol,1}$; i.e. $\mathbf{E}_{pol,2}^{+}\mathbf{E}_{pol,1} = 0$.

#204307 - $15.00 USD Received 6 Jan 2014; revised 13 Feb 2014; accepted 13 Feb 2014; published 1 Apr 2014

Using normalized Stokes vectors (**S** instead of **E**, with unchanged indices), we can write

$$RI = (1/2)\left(1+\mathbf{S}_{pol,1}^{T}\mathbf{S}_S\right) = (1/2)(1+\cos\delta) = \cos^2(\delta/2), \qquad RIE = 1-RI = \sin^2(\delta/2), \quad (1)$$

where T means the transpose and δ, the polarization error, is the angle between $\mathbf{S}_S$ and $\mathbf{S}_{pol,1}$ on the Poincaré sphere. *RI* measurements are directly influenced by intensity fluctuations. It is therefore better to measure the *RIE*. This is sketched in Fig. 1. From the *RIE* we can calculate the polarization error $\delta = 2\arcsin\sqrt{RIE} \approx 2\sqrt{RIE}$. The approximation holds for small δ.

This polarization error detection is widely in use and has enabled polarization tracking with very high accuracy up to 100 krad/s on the Poincaré sphere [3].

Ideally, the *RIE* would be the same as the polarization extinction ratio (PER). The *RIE* includes the controller circuit noise, namely measurement noise, while the true optical PER excludes it. Of course mean *RIE* and PER differ from the maximum ones, which is visible in the later Figs. 14–17, 20, and 21.

In all our experiments, *RIE* (just as PER) includes the polarization errors introduced by dithering the electrode voltages.

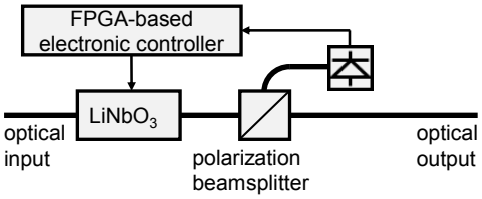

Fig. 1. Polarization controller with optical power measurement in cross polarization.

2.2 Electrical power in coherent receiver

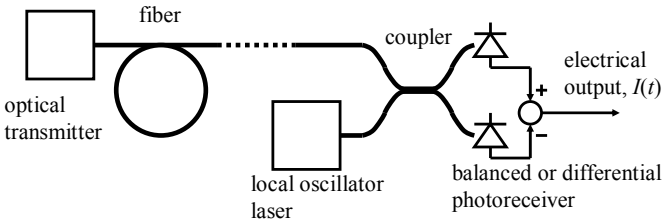

Fig. 2. Coherent optical transmission setup.

A very similar scenario occurs in coherent receivers (Fig. 2). With normalized signal and local oscillator fields $\mathbf{E}_S = \mathbf{E}_{S,0}e^{j\omega_S t}$, $\mathbf{E}_{LO} = j\mathbf{E}_{LO,0}e^{j\omega_{LO}t}$, the electrical AC signal power in the coherent receiver is proportional to the relative intensity

$$RI = \left|\mathbf{E}_{LO,0}^{+}\mathbf{E}_{S,0}\right|^2 = (1/2)\left(1+\mathbf{S}_{LO}^{T}\mathbf{S}_S\right) = \cos^2(\delta/2), \quad (2)$$

where δ is the angle between signal polarization $\mathbf{S}_S$ and local oscillator polarization $\mathbf{S}_{LO}$ on the Poincaré sphere. It behaves like the optical power behind a polarizer. As a consequence, the error signal in the configuration of Fig. 3 can be the electrical power measured in a coherent receiver of Fig. 2.

#204307 - $15.00 USD Received 6 Jan 2014; revised 13 Feb 2014; accepted 13 Feb 2014; published 1 Apr 2014

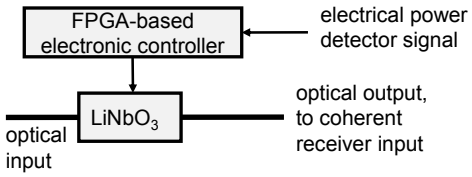

Fig. 3. Simplified block diagram of polarization controller suitable for electrical power measurement in coherent receiver.

2.3 Interference detection of polarization-multiplexed DQPSK and QAM signals

The foregoing possibilities are applicable for single-polarization signals. In contrast, the present scenario is for polarization-multiplexed (= dual-polarization = PDM) DQPSK signals which form an unpolarized sum signal $\mathbf{E}_S = \mathbf{E}_{S,1} + \mathbf{E}_{S,2} = c_1\mathbf{E}_{S,1,0} + c_2\mathbf{E}_{S,2,0}$. All the same the polarization channel signals $\mathbf{E}_{S,1} = c_1\mathbf{E}_{S,1,0}$, $\mathbf{E}_{S,2} = c_2\mathbf{E}_{S,2,0}$ can be separated. The polarization channels should be orthogonal to each other, $\mathbf{E}_{S,2}^{+}\mathbf{E}_{S,1} = 0$. $\mathbf{E}_{S,1,0}$, $\mathbf{E}_{S,2,0}$ are unmodulated optical carriers, usually from the same optical source. The modulated polarization channel signals have no carriers because the complex modulation symbols $c_1 = e^{j\phi_1}(\pm 1 \pm j)/\sqrt{2}$, $c_2 = e^{j\phi_2}(\pm 1 \pm j)/\sqrt{2}$ have zero means $\langle c_1 \rangle = 0$, $\langle c_2 \rangle = 0$. They also are uncorrelated, $\langle c_2^{*} c_1 \rangle = 0$. The angled brackets mean expectation value, the star denotes the complex conjugate, and ϕ_1, ϕ_2 are individual phases of the polarization channels.

At one PBS output (Fig. 4) the optical signal is fully polarized with an amplitude proportional to $\mathbf{E}_{pol,1}^{+}\mathbf{E}_S$. Its power equals

$$P_1 = \frac{1}{2}\left|\mathbf{E}_{pol,1}^{+}\mathbf{E}_S\right|^2 = \frac{1}{2}\left(\left|\mathbf{E}_{pol,1}^{+}\mathbf{E}_{S,1}\right|^2 + 2\,\mathrm{Re}\left(\left(\mathbf{E}_{pol,1}^{+}\mathbf{E}_{S,1}\right)\left(\mathbf{E}_{pol,1}^{+}\mathbf{E}_{S,2}\right)^{*}\right) + \left|\mathbf{E}_{pol,1}^{+}\mathbf{E}_{S,2}\right|^2\right). \tag{3}$$

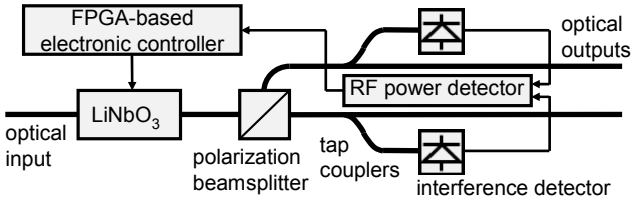

Fig. 4. Simplified block diagram of polarization controller with interference detection of polarization-multiplexed DQPSK signals.

We assume orthonormal $\mathbf{E}_{pol,1}$, $\mathbf{E}_{pol,2}$. Terms $\frac{1}{2}\left|\mathbf{E}_{S,i}\right|^2 = P_{S,i}$ $(i = 1,2)$ are constant, identical channel powers $P_{S,1} = P_{S,2} = P_S/2$, each equal to half the total signal power P_S. The expectation value of P_1 is $\langle P_1 \rangle = \frac{1}{2}\left(\left|\mathbf{E}_{pol,1}^{+}\mathbf{E}_{S,1}\right|^2 + \left|\mathbf{E}_{pol,1}^{+}\mathbf{E}_{S,2}\right|^2\right) = P_S/2$. Now we substitute $\mathbf{E}_{pol,1}^{+}\mathbf{E}_{S,i} = \sqrt{2P_{S,i}}\,e^{j\arg\left(\mathbf{E}_{pol,1}^{+}\mathbf{E}_{S,i}\right)}\cos\left(\delta_i/2\right)$. The angles δ_i on the Poincaré sphere between the 1st transmitted polarizer eigenstate and the polarization channel signal *i* obey $\delta_1 + \delta_2 = \pi$. Accordingly, the AC part of the optical power is

#204307 - $15.00 USD Received 6 Jan 2014; revised 13 Feb 2014; accepted 13 Feb 2014; published 1 Apr 2014

$$P_{1,AC} = P_1 - \langle P_1 \rangle = 2\sqrt{P_{S,1}P_{S,2}}\cos(\delta_1/2)\cos(\delta_2/2)\cos(\psi) = (P_S/2)\sin(\delta_1)\cos(\psi) \quad (4)$$

with $\psi = \arg\left(\left(\mathbf{E}^+_{pol,1}\mathbf{E}_{S,1}\right)\left(\mathbf{E}^+_{pol,1}\mathbf{E}_{S,2}\right)^*\right)$. The uncorrelated DQPSK modulations let ψ jump from symbol to symbol by multiples of $\pi/2$ through all 4 quadrants, yielding $\langle \cos^2\psi \rangle = 1/2$. At the other PBS output the signal amplitude is proportional to $\mathbf{E}^+_{pol,2}\mathbf{E}_S$, and the AC part of the respective power equals $P_{2,AC} = -P_{1,AC}$. This is evident because the total power is constant, $P_1 + P_2 = P_{S,1} + P_{S,2} = P_S = \frac{1}{2}|\mathbf{E}_S|^2$. It is possible to detect P_1, P_2 or their difference $P_1 - P_2$ in two photoreceivers. The AC part of the measured photocurrent or photocurrent difference is always proportional to $\sin\delta_1$. The expectation value of the electrical power, measured in a square-law power detector, is proportional to $\langle (\sin(\delta_1)\cos(\psi))^2 \rangle = (1/2)\sin^2\delta_1$ and to P_S^2. We can therefore define the relative intensity error as

$$RIE = \sin^2\delta_1. \quad (5)$$

This is similar to *RIE* in (1) but a certain level of *RIE* requires only half as large a polarization mismatch angle ($\delta_1 = \delta/2$)! The reason for this is that there is not only one optimum polarization controller setting but also a second one in which the two demultiplexed polarization channels are exchanged.

The described interference detection scheme was first demonstrated in [13].

So far we have tacitly assumed NRZ signal format. In practice, the NRZ-DQPSK symbol transitions with non-zero duration generate amplitude noise which deteriorates the interference contrast.

The above calculation holds also for time-aligned RZ signals. The difference to NRZ is that the symbol transitions do not generate wideband amplitude noise. Rather there is a strong clock signal component in the photocurrents which is usually outside the bandwidth of the photoreceivers used for this interference detection. RZ signals hence yield a better interference contrast than NRZ signals.

QAM signals with independent zero-mean modulation in both quadratures, such as 16-QAM signals, can also be polarization-demultiplexed the same way. The difference to DQPSK signals is that there are more amplitude levels. The interference contrast is therefore decreased compared to DQPSK signals.

For time-interleaved RZ signals interference becomes much weaker. Fortunately, the receiver is also much less subject to interference.

In practice, an electrical power detector may not be truly quadratic and the measured intensity error can differ from the predicted one. Furthermore, the photoreceivers may go into saturation. We have quantified all this in a setup according to Fig. 4 with PIN photoreceivers, using a 40-Gbaud PDM-DQPSK (160 Gb/s) signal [13]. It is modulated independently with zero mean in both quadratures of both polarizations.

Figure 5 shows the maximum (= maximally achievable) intensity error, corresponding to $\sin^2\delta_1 = 1$, as a function of optical input power P_S at each photoreceiver. Signal polarizations were set accordingly. Also shown is the predicted behavior $\propto P_S^2$ for an ideal square-law power detector and $\propto P_S$ for an ideal linear amplitude detector. All curves are normalized to the value 1 at –4 dBm optical power. At low P_S, the measured maximum intensity error scales fairly $\propto P_S^2$ whereas at high P_S it scales more $\propto P_S$. This is a property of the used electrical high frequency power detector. In Fig. 6 the same information is displayed again, but in a double logarithmic plot.

#204307 - $15.00 USD Received 6 Jan 2014; revised 13 Feb 2014; accepted 13 Feb 2014; published 1 Apr 2014

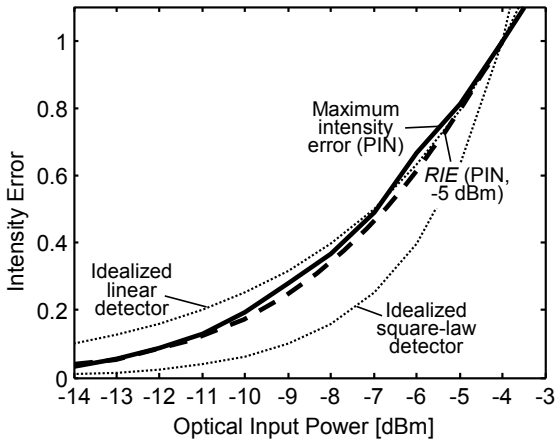

Fig. 5. Maximum intensity error, measured with maximum interference in PIN photoreceivers, as a function of optical input power, for 40 Gbaud PDM-DQPSK. Also shown is relative intensity error (*RIE*) at a constant −5 dBm optical input power as a function of polarization interference, expressed as an equivalent optical power. Note that all curves are normalized to the value 1 at −4 dBm optical power. Idealized quadratic and linear electrical detection is displayed for comparison.

We have repeated the experiment with a pure variation of the interference term $RIE = \sin^2 \delta_1$ at a constant optical power of −5 dBm. Angle δ_1 was quantified as follows: With a single-polarization signal and a polarimeter (Novoptel PM1000), those settings of a polarization scrambler (Novoptel EPS1000, here and in the other manuscript sections) were identified which resulted in certain angle distances δ_1 with respect to that point on the Poincaré sphere where one of the two polarization channels of a dual-polarization signal had to lie in order to minimize produced interference. These settings were then applied to the dual-polarization signal. The results are also shown in Fig. 5 (dashed). Here the horizontal axis means $10\log_{10}\left(\sin^2 \delta_1\right)$ − 4 dBm. The resulting *RIE* as a function of interference behaves similar as the maximum intensity error as a function of optical power. The slight differences between these two could be due to a beginning trend toward saturation at high optical power levels, due to photoreceiver overload.

2.4 Interference detection of polarization-multiplexed signals with other modulation formats

DPSK and duobinary signals are modulated in only one quadrature, like standard ASK signals. So the phase difference ψ between the polarization channels typically changes by 0 or π from symbol to symbol. This kind of modulation does not affect the electrical interference power which is proportional to $\cos^2 \psi = (1/2)(1+\cos(2\psi))$. Interference must therefore be adequately randomized. More precisely, $\langle \cos(2\psi) \rangle = 0$ must be achieved. ψ changes not only with modulation but also, additively, as a function of the static phase delay between the polarization channels. For interference randomization, the transmitter combines the two polarization channels with an optical delay difference τ, which is easily realized by fibers, and the transmitter laser frequency is sinusoidally modulated, in particular by a small pump current modulation (Fig. 7). Let the modulation frequency be $f = 1/T$ and the peak-to-peak deviation ΔF_{pp}. A momentary frequency excursion $F(t) = \frac{\Delta F_{pp}}{2} \sin\left(2\pi f\left(t+\tau/2\right)\right)$ yields a momentary optical phase excursion $\Psi(t) = \int 2\pi F(t)\, dt = -\frac{\Delta F_{pp}}{2f} \cos\left(2\pi f\left(t+\tau/2\right)\right)$.

#204307 - $15.00 USD Received 6 Jan 2014; revised 13 Feb 2014; accepted 13 Feb 2014; published 1 Apr 2014

Leaving aside the data modulation which has no effect on $\cos(2\psi)$, the doubled angle difference between the two polarization channels equals $2\psi(t) = 2\left(\Psi(t) - \Psi(t-\tau)\right) = 2\eta\sin(2\pi ft)$ with angular modulation index $2\eta = 2\pi\,\Delta F_{pp}\,\tau\,\mathrm{sinc}(\pi f\tau)$. For $\langle\cos(2\psi)\rangle = 0$, $J_0(2\eta) = 0$ is required. This is fulfilled if one sets $\Delta F_{pp} = \dfrac{1.202}{\pi\tau\,\mathrm{sinc}(\pi f\tau)}$. The frequency $f = 1/T$ is chosen to match the averaging time *T* of the RF interference detector. More details are described in [7]. Figure 5 applies also here.

Like DPSK and duobinary signals, ASK signals are modulated in only one quadrature. But they have an optical carrier. This avoids the need of broadband RF power detection. Rather, interference can be detected at low frequencies. The interference phase must again be randomized. The procedure to be undertaken is similar to above, but higher-order Bessel lines must be detected, at least one even and one odd line. Details are described in [28]. RZ-ASK and CSRZ-ASK are likewise possible.

3. Interference detection with avalanche diode photoreceivers

3.1 Principle and its realization

The schematic of Fig. 4 is usually realized with PIN diode photoreceivers. As can be seen from Fig. 5, the maximum intensity error varies strongly as a function of optical signal power P_S. This crucially affects control quality, with too high P_S causing instability and low P_S reducing tracking speed. The problem can be solved by automatic gain control with an optical preamplifier. However, this costs extra and is not always available.

As a simple alternative solution we have replaced the PIN photodiodes in Fig. 4 by avalanche photodiodes (APDs). The basic idea is to operate the APD with a constant current. If no signal is available the reverse APD voltage is high. With signal it becomes lower. For a given APD current with constant mean its undulations caused by interference should also have constant amplitude. However, this holds only if the gain-bandwidth-product of the APD is infinite. A 10-GHz APD photoreceiver is gain-bandwidth limited to quite some extent. So, the APD current should be smaller if optical signal is strong and larger if optical power is weak. This can be realized if the APD reverse voltage supply has a negative impedance.

The principle was tested using 40-Gbaud PDM-DQPSK, like in Fig. 5. The APDs had separate reverse voltage sources, since at a given wanted current some voltage variation may be expected between different devices. For a photocurrent I_{APD} the reverse voltage is $V_{APD} = V_0 - R\cdot I_{APD}$. After some experiments we chose the inner impedance *R* of each APD power supply to be *R* = −180 kΩ (negative impedance), and the open-source voltages equal to V_0 = −1.6 V. The circuits can supply only values $V_{APD} \geq 0$. We operated between V_{APD} = 27.6 V, I_{APD} = 0.161 mA at P_S = −26 dBm (*M* = 76) and V_{APD} = 21.6 V, I_{APD} = 0.128 mA at P_S = −15 dBm optical input power (*M* = 4.8). The APD multiplication factors *M* are given under the assumption of a responsivity of 0.85 A/W at *M* = 1.

For this configuration, Fig. 6 shows maximum achievable intensity error in dB as function of optical input power. In a 7-dB optical power tolerance range between −22 dBm and −15 dBm, it stays between 0.5 (−3 dB) and 1 (0 dB), with a maximum of 1 at −16 dBm. When input power exceeds −15 dBm, sensitivity decreases due to APD diode overload. Included for comparison is the maximum intensity error data of Fig. 5, obtained with PIN photoreceivers. For those, the optical power tolerance range is only 3 dB, between −7 dBm and −4 dBm (top x-axis). This shows that, based on an exemplary allowed *RIE* reduction of ~3 dB, the available input power range is more than doubled when using the APD instead of

#204307 - $15.00 USD Received 6 Jan 2014; revised 13 Feb 2014; accepted 13 Feb 2014; published 1 Apr 2014

the PIN photoreceivers. Sensitivity at the upper end of the optical power tolerance range is 12 dB better for the APD compared to the PIN photoreceivers.

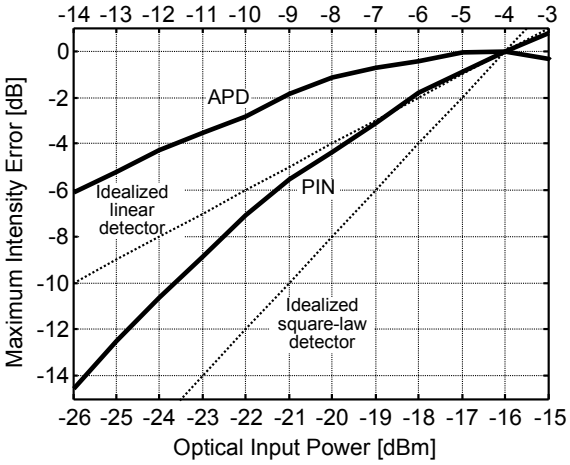

Fig. 6. Maximum (solid curve) achievable *RIE* using APD as function of optical input power, for 40 Gbaud PDM-DQPSK. This is compared with maximum *RIE* using PIN photodiodes. X-Axes are shown for PIN (top) and APD (bottom) photoreceivers.

3.2 Transmission experiment

To test PDM transmission with interference detection in APD photoreceivers we put these into our earlier 10-Gbaud PDM-RZ-DPSK (20 Gb/s) setup [7] (Fig. 7). DPSK polarization channel interference was randomized as described in Section 2.4. The polarization scrambler generated the polarization fluctuations to be tracked. To this purpose, the scrambler drives the control voltages of a $LiNbO_3$ polarization transformer to act as a fast rotating halfwave plate (HWP) between two trios of quarterwave plates (QWPs), the latter rotating at slower, incommensurate rates. This generates circles on the Poincaré sphere with varying sizes and orientations, which comprises many reiterating worst-case trajectories that are difficult to track by a polarization controller. Scrambling speed is maximum if the HWP input polarization is linear. Mean scrambling speed is $\pi/4$ times the maximum one.

The signal was transmitted over 430 km in 5 fiber spans. Then, polarization was stabilized in a second $LiNbO_3$ polarization transformer (EOSPACE PC) which is part of a polarization controller (Novoptel EPC1000, here and in the other manuscript sections). A gradient descent algorithm, implemented in the controller FPGA, acts on the electrode voltages and aims at minimizing the feedback signal provided by the interference detector. For the function it does not matter whether the $LiNbO_3$ output fiber is standard (SSMF) or polarization-maintaining (PMF). Here it was SSMF.

#204307 - $15.00 USD Received 6 Jan 2014; revised 13 Feb 2014; accepted 13 Feb 2014; published 1 Apr 2014

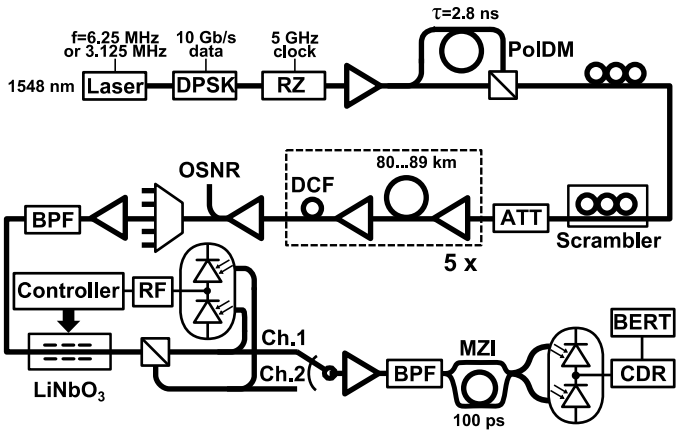

Fig. 7. Setup for 20-Gb/s PDM-RZ-DPSK transmission. An endless, electrooptic polarization controller with interference detection demultiplexes the two polarization channels, enabling subsequent direct detection.

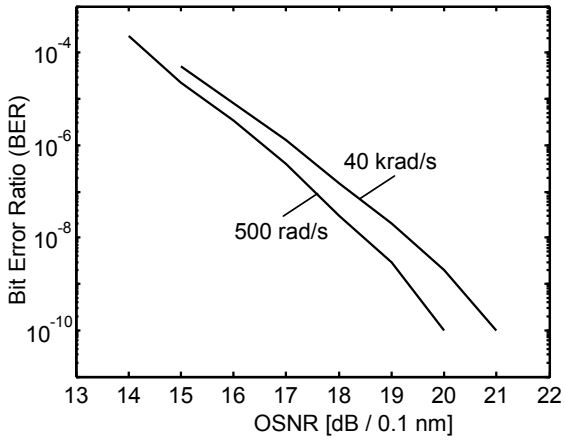

Fig. 8. BER as function of optical signal-to-noise ratio at 500 rad/s and 40 krad/s scrambling.

Without the fiber link, the attenuation after the scrambler was adjusted to set specific optical signal-to-noise ratio (OSNR) values. Figure 8 shows the bit error ratio (BER) as a function of the OSNR. The two curves show measurements at 500 rad/s and 40 krad/s maximum scrambling speed. Both demultiplexer outputs showed similar results. With an OSNR exceeding 20 dB (21 dB) in a 0.1 nm bandwidth, transmission was error-free at 500 rad/s (40 krad/s) scrambling speed. The high scrambling speed required the OSNR to be increased by ~1 dB at low BER and ~0.5 dB at high BER.

Next, receiver sensitivity was tested at two different OSNRs over a 9 dB input power range, see Fig. 9. BER increased from $1\cdot10^{-8}$ to $3.6\cdot10^{-8}$ and from $1\cdot10^{-6}$ to $3\cdot10^{-6}$ at 500 rad/s scrambling and from $1.8\cdot10^{-8}$ to $2.3\cdot10^{-7}$ and from $1.6\cdot10^{-7}$ to $1\cdot10^{-5}$ at 40 krad/s scrambling when the input power was decreased from −15 dBm to −24 dBm. A 6-dB power change hardly affects the BER, and even the 9-dB power reduction increases the BER by only one decade. For high multiplication factors, APDs not only become bandwidth-limited but also contribute excess noise. Both effects contribute to the observed moderate BER increases upon input power reduction and seem to be undramatic in our experiment.

#204307 - $15.00 USD Received 6 Jan 2014; revised 13 Feb 2014; accepted 13 Feb 2014; published 1 Apr 2014

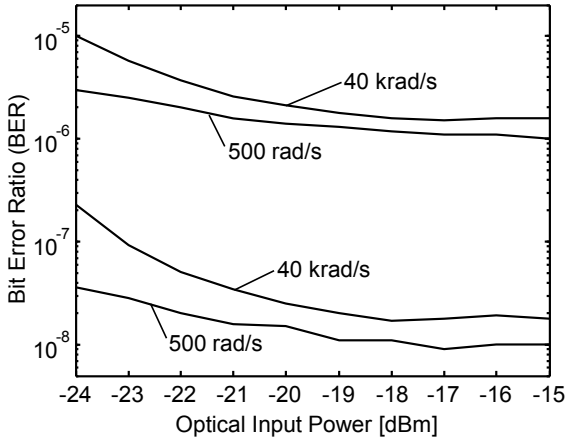

Fig. 9. BER as function of optical input power for 500 rad/s and 40 krad/s scrambling, starting for two different OSNRs which yielded BER 10^{-6} and 10^{-8} at 500 rad/s and −15 dBm input power.

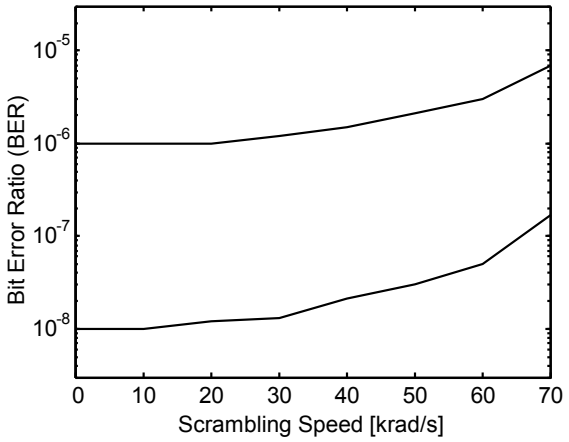

Fig. 10. BER as function of maximum scrambling speed, starting from BER 10^{-6} and 10^{-8}.

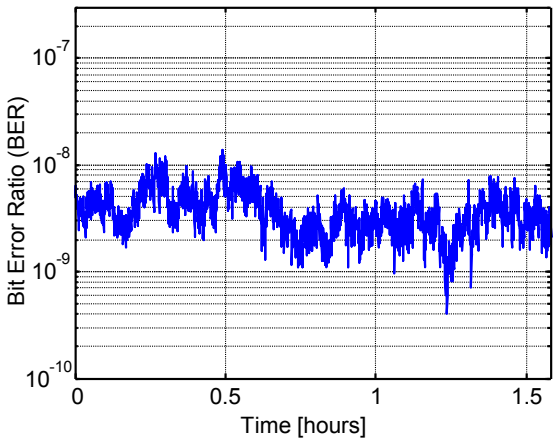

Fig. 11. BER over > 1.5 hours after transmission over 430 km with 40 krad/s scrambling.

#204307 - $15.00 USD Received 6 Jan 2014; revised 13 Feb 2014; accepted 13 Feb 2014; published 1 Apr 2014

The influence of scrambling speed on the BER is shown in Fig. 10. Starting at BERs of 10^{-8} and 10^{-6}, scrambling speed was increased in 10-krad/s steps. BERs of $2.1 \cdot 10^{-8}$ and $1.5 \cdot 10^{-6}$ were reached at 40 krad/s scrambling. At a maximum scrambling speed of 70 krad/s, BERs reached $1.7 \cdot 10^{-7}$ and $7 \cdot 10^{-6}$.

Finally, the 430 km fiber link was inserted into the setup. At maximum OSNR, transmission was error-free. OSNR was decreased to obtain a BER between 10^{-9} and 10^{-8}. The BER was recorded in intervals of 2 s. Within a measurement time of >1.5 hours, BER showed fluctuations within about 1 decade, see Fig. 11.

4. High-precision endless polarization control

4.1 Experimental setup

For many transmission links, expected polarization changes are comparatively slow. For this and many lab applications, ultimate polarization tracking speed can partly be sacrificed in order to achieve higher crosstalk suppression at moderate tracking speed. Ultimate crosstalk suppression is needed for higher-order PDM-QAM or similar modulation schemes. To achieve this, we optimize the control quality of a fast polarization demultiplexer and thereby reduced its tracking speed to a target of 1000 rad/s, which still covers manual fiber handling. We have previously found that our speeds for single- and dual-polarization tracking are almost equal [6]. Here we have chosen single-polarization tracking because the optical power of the cross-polarized signal is most suitable for accurate and meaningful *RIE* recording.

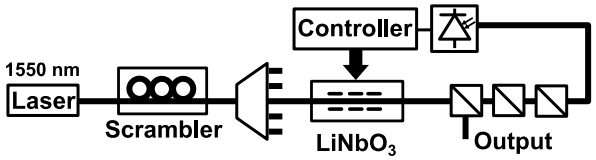

Fig. 12. Setup for high-precision polarization control.

In our setup (Fig. 12), the polarization scrambler impresses arbitrary, endless polarization changes on the signal of a 1550 nm DFB laser. The QWPs of the scrambler are configured to generate a maximum of 50 rad/s. The HWP, which is configured to generate 1000 rad/s, could optionally be included. Important for the following experiments is the quasi-continuous polarization transformation of the scrambler: New polarization states are set every 40 ns, which leads, DAC quantization excluded, to a granularity of only 40 µrad at the target scrambling speed of 1000 rad/s.

The scrambled signal is fed through a DWDM DEMUX filter to improve side mode suppression of the laser signal. The polarization of the filtered signal is then stabilized in front of a PBS like in the experiment described before. The output fiber of the $LiNbO_3$ polarization transformer is SSMF. The subsequent PBS made with PMF provides an extinction ratio of about 24 dB. Hence it is unsuitable for measuring large extinctions because the through signal is partly leaked, with through polarization, to that PBS output where only the cross-polarized signal should appear. The through polarization extinction at the cross polarization PBS output is therefore improved to >50 dB by two additional polarizers placed between PBS and photodiode. These are connected via PMF to ensure correct alignment.

The error signal of the PBS is detected by a photodiode and sampled by the controller. An *RIE* of 1 refers to the maximum optical output power of −10 dBm.

Note that if the polarization transformer outputs only through polarization and no cross polarization then the extinction is infinite even without PBS. Hence the additional polarizers do not increase polarization extinction. They simply allow measuring the achieved extinction with higher accuracy. The situation would be different for dual-polarization demultiplexing: Additional polarizers would have to be inserted right at the PBS outputs, even before the tap couplers of Fig. 4, in order to suppress the feedthrough components with wrong polarizations.

#204307 - $15.00 USD Received 6 Jan 2014; revised 13 Feb 2014; accepted 13 Feb 2014; published 1 Apr 2014

4.2 Control parameters

It has been shown before [6] that mean and maximum polarization errors of the polarization controller depend on dithering depth. When slow polarization changes are tracked, large dithering depth increases mean polarization errors. On the other hand, very fast polarization changes cannot be accurately tracked when dithering depth is too small. As a first measure, we optimize dithering depth for the targeted tracking speed.

As a second measure, when expected polarization changes are relatively slow, the drawback of a smaller dithering depth can partly be compensated by longer averaging times during sampling of the feedback signal at the dither modulation points. Table 1 shows the relation between sample averaging time and iteration time of the controller. We introduce the averaging time exponent (ATE) to label the different configurations. At ATE = 6, the averaging time is increased by a factor of 64, while the iteration time is increased by a factor of about 28. The reduced control speed is still high enough to track polarization changes in the low krad/s range.

In the polarization control algorithm there is a pullback speed for the voltages of $LiNbO_3$ polarization transformer sections which are driven near the breakdown limit. Typically we set it so that it is fast enough for tracking 40, 60 or 100 krad/s. This would be too fast here, since dithering depth is reduced and averaging time is increased, which prevents other sections to take over fast enough the function of the section under voltage pullback. As a third measure, we have hence reduced the voltage pullback speed to suffice for tracking at 2...3 krad/s.

Table 1. Control iteration times, depending on *RIE* feedback sample averaging times

Averaging Time Exponent (ATE)	Averaging Time	Iteration Time
0	0.08 µs	1.1 µs
1	0.16 µs	1.6 µs
2	0.32 µs	2.5 µs
3	0.64 µs	4.4 µs
4	1.28 µs	8.3 µs
5	2.56 µs	16 µs
6	5.12 µs	31 µs

4.3 Experimental results

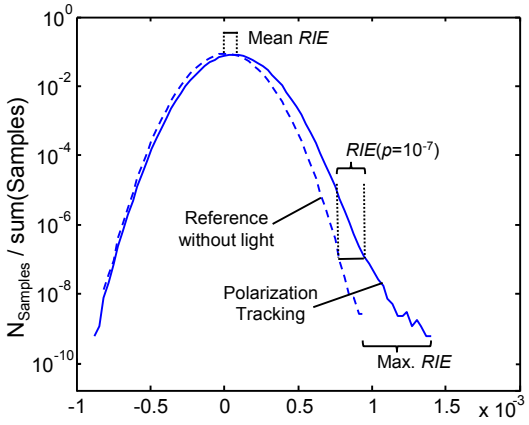

Fig. 13. Definition of polarization errors, shown at sample histograms of relative intensity error (*RIE*). Histogram bin width is $\Delta RIE = 3.3 \cdot 10^{-5}$.

For analysis of tracking accuracy, samples of the feedback signal are cumulated in histograms at a rate of 5.5 MHz during control (Fig. 13). Each histogram bin has a width of $\Delta RIE = 3.3 \cdot 10^{-5}$. A reference measurement without light is also taken. The mean *RIE* is the mean value of all *RIE* samples recorded while tracking. An appropriate offset is subtracted so

#204307 - $15.00 USD Received 6 Jan 2014; revised 13 Feb 2014; accepted 13 Feb 2014; published 1 Apr 2014

that the mean *RIE* of a reference measurement without light becomes 0. The maximum *RIE* is defined as the difference between the maximum relative intensity value of all taken samples in the tracking experiment and in the reference measurement. Since the probability of the maximum error sample is very low, its value differs randomly in consecutive measurements. To get a more repeatable measure of large *RIE*s, we additionally analyze the difference between the positive *RIE*s at the point where probability of occurrence drops below 10^{-7} in a $\Delta RIE = 3.3 \cdot 10^{-5}$ bin.

Figures 14, 15, and 16 show analysis of polarization errors $\delta = 2\arcsin\sqrt{RIE} \approx 2\sqrt{RIE}$, derived from *RIE*s for 50%, 38% and 25% dithering depth. 100% dithering depth refers to an rms electrode dither voltage of ~0.45 Volt, as usually selected for high-speed tracking. The utilized *RIE* values are determined as depicted in Fig. 13 by comparing *RIE* distributions under tracking and without light for three different occurrence probabilities: Figs. 14, 15, and 16 show mean and maximum polarization errors in rad as well as the polarization errors at the above-defined 10^{-7} probability threshold of *RIE*. Measurements at ATEs between 0 and 6 are shown for 50 rad/s (solid lines) and 1000 rad/s (dashed lines) scrambling speed.

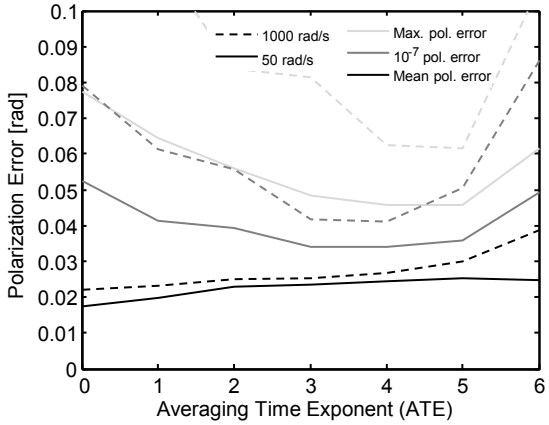

Fig. 14. Mean and maximum polarization errors at 50% dithering.

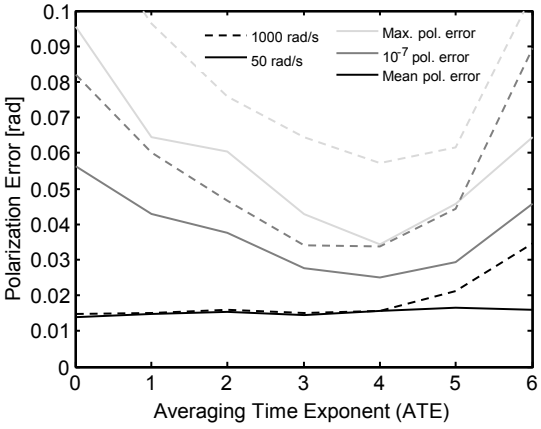

Fig. 15. Mean and maximum polarization errors at 38% dithering.

At 50% dithering, mean errors increase with rising ATE, whereas they decrease with rising ATE at 25% dithering. This implies that polarization errors due to dithering dominate the mean error at 50% dithering. Longer averaging is not helpful in this case. At 25% dithering, mean errors are dominated by random displacements of the controller's operating

#204307 - $15.00 USD Received 6 Jan 2014; revised 13 Feb 2014; accepted 13 Feb 2014; published 1 Apr 2014

point due to the imprecise gradient determination. In this case, increasing the ATE brought the mean error from 0.027 rad down to 0.02 rad at 50 rad/s scrambling. At 1000 rad/s scrambling, mean errors suffer from reduced tracking speed at ATE > 4 at all dithering depths. 1000 rad/s means a polarization variance of already 0.031 rad per iteration (31 μs) if ATE is chosen as large as ATE = 6.

38% dithering at ATE = 4 was found to be a good compromise, since it provides a mean polarization error below 0.02 rad at both 50 rad/s and 1000 rad/s polarization changes. A polarization error of 0.02 rad refers to a *RIE* of $1 \cdot 10^{-4}$ and a crosstalk attenuation of 40 dB.

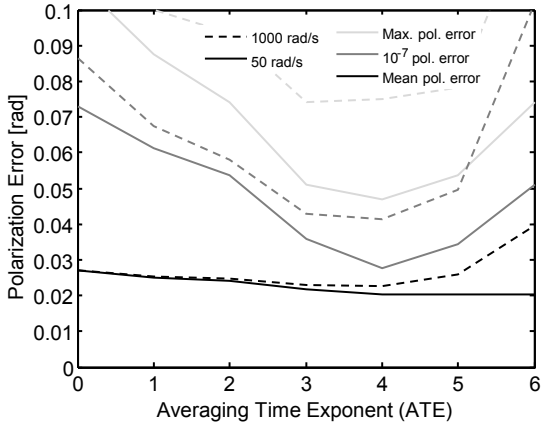

Fig. 16. Mean and maximum polarization errors at 25% dithering.

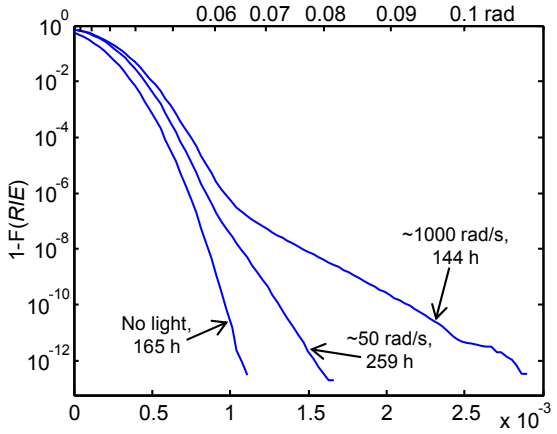

Fig. 17. Inverse cumulative distribution function of Relative Intensity Error (*RIE*) during long term measurements with 38% dithering and ATE = 4 at 50 and 1000 rad/s scrambling speeds.

In this configuration, two long-time histograms were recorded. The inverse cumulative distribution function 1–F(*RIE*) has been derived from the histograms, see Fig. 17. The graphs show the probability that a given sample exceeds the value on the abscissa. It is 0.5 for *RIE* = 0 in the reference measurement and between 0.5 and 0 in the tracking experiments depending on *RIE* distribution. Note that the vertical axis is not directly comparable to that of Fig. 13.

Polarization changes of 50 rad/s speed were tracked over 259 hours, with a difference in the maximum *RIE*s with and without light of ~$6 \cdot 10^{-4}$ (–32.2 dB attenuation, probability $<10^{-12}$). The derived maximum polarization error was 0.049 rad. At 1000 rad/s scrambling, maximum *RIE* difference was $1.8 \cdot 10^{-3}$ during 144 hours. This refers to a maximum

#204307 - $15.00 USD Received 6 Jan 2014; revised 13 Feb 2014; accepted 13 Feb 2014; published 1 Apr 2014

polarization error of 0.085 rad (−27.4 dB attenuation, probability $<10^{-12}$). In both cases, mean crosstalk extinction was >40 dB. This value correctly includes the finite extinction introduced by electrode voltage dithering. We predicted the latter extinction to be also >40 dB.

In the setup of Fig. 1 or 12, higher *RIE* cannot be distinguished from higher optical input power. Automatic gain control of (control-theoretical) feedback type, for example by an APD whose voltage is changed as a function of current (even by a serial resistor), is therefore difficult or impossible: For good dynamic behavior and tracking speed, gradient steps should be proportional to measured *RIE* variations. This becomes impossible if the mean *RIE* (strongly related to the *RIE* variations!) is automatically controlled to be constant.

On the other hand, an APD with fixed voltage should scale the optical power to lower levels according to the multiplication factor. An additional optical power measurement before the PBS should allow adjusting the APD voltage or, more generally, correctly interpreting and scaling the photocurrent behind the PBS in a feedforward automatic gain control.

5. 1-THz bandwidth endless polarization control

5.1 Experimental setup

Figure 18 shows the setup of our polarization tracking experiment for large optical bandwidth. 11 tunable laser sources are adjusted to frequencies between 192.8 and 193.8 THz in a 100-GHz grid. The laser signals are fed into 11 inputs of a 16x1 fiber coupler. Each laser signal is manually polarization-aligned to the transmitted eigenmode of a subsequent polarizer. The optical output powers of the lasers are matched to produce equal peaks in the optical spectrum of the combined signal (Fig. 19). After impressing fast and endless polarization changes by one of our polarization scramblers, we re-stabilize the polarization of the broadband signal at the input of a PBS. The $LiNbO_3$ polarization transformer has PMF at its output. The main PBS output carries the re-polarized signal. The optical power at the other PBS output is detected by a photodiode as described in Section 2.1. The photocurrent provides the feedback signal for the $LiNbO_3$ polarization transformer and is minimized in a gradient descent algorithm under control. Suitably normalized it becomes the relative intensity error (*RIE*).

We assess the achievable extinction in the presence of polarization mode dispersion (PMD). In (1), $\delta = 2\pi f\tau$ can apply as a worst case, where f is the frequency offset from the optical center frequency and τ is the differential group delay (DGD). If spectral density is uniform the worst-case irreducible overall $RIE_{\min}$ is obtained by averaging *RIE* over the total bandwidth Δf, from $f = -\Delta f/2$ to $f = \Delta f/2$. For small $\Delta f\tau$ we obtain $RIE_{\min} \approx (\pi\Delta f\tau)^2/12$.

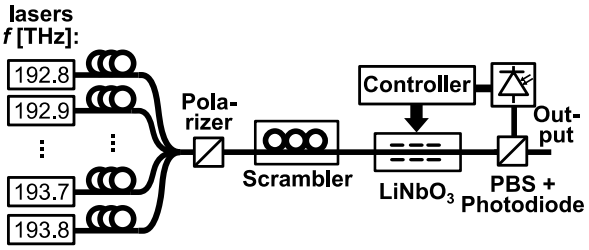

Fig. 18. Setup for polarization control with 1 THz bandwidth, including fast polarization scrambling for testing purposes.

Another issue is the quality of the signals and their relevance for dual-polarization tracking. As mentioned before, single- vs. dual-polarization tracking speeds are similar [6]. But as per Section 2.3, interference is broadband whereas our 11 optical signals interfere only with 100 GHz and multiples thereof. So we need to assess the required bandwidth of interference detection. While in [5] an electrical bandwidth of about 7 GHz was sufficient for 50 Gbaud polarization demultiplexing, available photoreceivers and electronic technology promise a conveniently achievable electrical bandwidth of about 40 GHz. Such an

#204307 - $15.00 USD Received 6 Jan 2014; revised 13 Feb 2014; accepted 13 Feb 2014; published 1 Apr 2014

interference detector would be fine for a scaled symbol rate of 286 Gbaud. For a 1-THz optical bandwidth another electrical bandwidth factor of 3.5 is hence missing. But this can easily be covered and circumvented by more averaging of the detected interference and slower polarization tracking, presumably still reaching at least 20 krad/s (3.5 times slower than now).

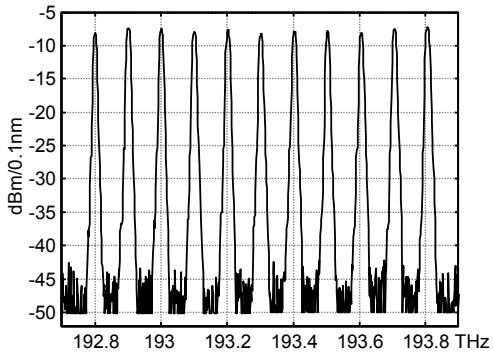

Fig. 19. Optical spectrum of 11 equispaced laser signals with a total bandwidth of 1 THz.

5.2 Experimental results

The extinction at the output port of the setup was verified with an optical power meter. When the controller was switched from feedback minimization to maximization at low scrambling speed, the main output power dropped by 24.75 dB. This reveals a mean *RIE* of 0.33% under control. Before, with a single laser frequency sweep over 5 THz and a polarimeter, DGD of the scrambler alone without applied voltages was determined to be 55 fs. This yields, in the worst case, an $RIE_{\min} \approx (\pi \Delta f \tau)^2 / 12$ of already 0.25%. However, when the scrambler is operated it may partly compensate its $LiNbO_3$ waveguide PMD. The DGD of the controller possibly adds to the 55 fs. It could not be determined exactly, because output of the $LiNbO_3$ element inside the controller is directly connected to a polarization maintaining fiber.

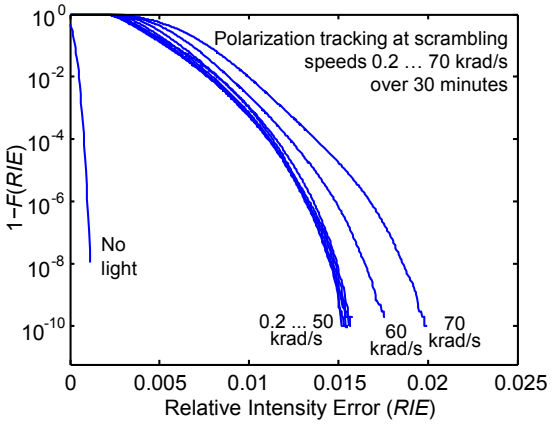

Fig. 20. Complementary cumulative distribution function 1–F(*RIE*) of relative intensity error (*RIE*) for various polarization scrambling speeds.

For accurate error analysis, samples of the *RIE* were accumulated into histograms inside the controller at a rate of 6.7 MS/s during control. Figure 20 shows complementary distribution functions 1–F(*RIE*), derived from the *RIE* histograms. Every curve shows one of eight 30-minute long measurements, at defined maximum polarization scrambling speeds of

#204307 - $15.00 USD Received 6 Jan 2014; revised 13 Feb 2014; accepted 13 Feb 2014; published 1 Apr 2014

0.2, 10, 20, ..., 70 krad/s. The leftmost curve shows a reference measurement without light to determine the zero point *RIE* = 0. As expected, the measurements with light are shifted to the right due to finite extinction caused by PMD. Up to a scrambling speed of 50 krad/s, the maximum *RIE*s depend largely on PMD, not on scrambling speed, and do not exceed 1.6%.

Figure 21 shows those *RIE*s which are surpassed with probabilities 0.5 (mean *RIE*), 10^{-3}, 10^{-6} and 0 (maximum *RIE*) as a function of scrambling speed. The mean *RIE*s at scrambling speeds 200 rad/s (0.349%), 10 krad/s (0.335%) and 20 krad/s (0.346%) comply with the extinction measured by hand. Beyond, mean *RIE* increases up to 0.525% at 70 krad/s scrambling speed. The corresponding extinction is 22.8 dB, just 2 dB less than at slow scrambling speeds.

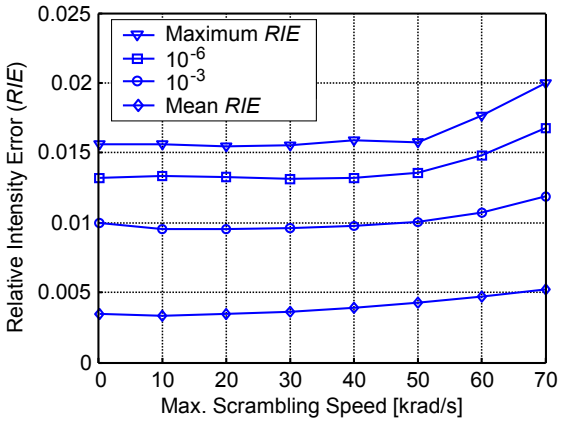

Fig. 21. Relative intensity error (*RIE*) surpassed with certain probabilities as a function of polarization scrambling speed.

6. Discussion and conclusion

We have shown how, for a variety of applications and modulation formats, suitable error signals can be obtained for optical polarization trackers and demultiplexers. Interference detection in various embodiments is very well suited for modulated dual-polarization signals. Regarding experiments, we summarize:

(i) For PIN photoreceivers, interference detected with an electrical power detector yields an optical power tolerance range of 3 dB. With APD photoreceivers having avalanche voltage supplies with negative inner resistance, this range is extended to 7 dB while the sensitivity is improved by 12 dB. Using APD photoreceivers we have transmitted a 20-Gb/s PDM-DPSK signal over 430 km and tracked polarization fluctuations at up to 70 krad/s speed.

(ii) At much lower tracking speeds we have furthermore assessed the achievable control quality. By proper control parameter setting and aided by polarizers and PBS we have demonstrated a mean crosstalk suppression of >40 dB while tracking endless polarization changes of up to 1000 rad/s speed. Two extended measurements show longterm stability with minimum momentary crosstalk suppressions of 32.2 dB (50 rad/s) and 27.4 dB (1000 rad/s).

(iii) Finally we have shown that endless polarization control is possible with a 1 THz optical bandwidth. This is >20 times wider than electronically possible in coherent receivers. Maximum tracking speed is again 70 krad/s, by far sufficient for tracking arising polarization fluctuations. Polarization fluctuations up to 50 krad/s even hardly have any effect. PMD of the polarization scrambler used for test purposes was on the order of 55 fs.

These experiments and others cited prove versatile, accurate, fast polarization tracking with electrooptic $LiNbO_3$ polarization transformers.

#204307 - $15.00 USD Received 6 Jan 2014; revised 13 Feb 2014; accepted 13 Feb 2014; published 1 Apr 2014